ADVANCED MATERIALS
www.advmat.de

Cucurbit[8]uril Mediated Supramolecular and Photocrosslinked Interpenetrating Network Hydrogel Matrices for 3D-Bioprinting

Yuqing Wang, Alexander Matthias Bimmermann, Meik Neufurth, and Pol Besenius**

Printing of biologically functional constructs is significant for applications in tissue engineering and regenerative medicine. Designing bioinks remains remarkably challenging due to the multifaceted requirements in terms of the physical, chemical, and biochemical properties of the three-dimensional matrix, such as cytocompatibility, printability, and shape fidelity. In order to promote matrix and materials stiffness, while not sacrificing stress relaxation mechanisms which support cell spreading, migration, and differentiation, this work reports an interpenetrating network (IPN) bioink design. The approach makes use of a chemically defined network, combining physical and chemical crosslinking units with a tunable composition and network density, as well as spatiotemporal control over post-assembly material stiffening. To this end, star-shaped poly(ethylene glycol)s functionalized with Phe-Gly-Gly tripeptide or photoactive stilbazolium are synthesized, and used to prepare three-dimensional networks with cucurbit[8]uril (CB[8]) through supramolecular host–guest complexation. The hydrogel obtained shows fast relaxation and thus supports the proliferation and differentiation of cells. Upon irradiation, the mechanical properties of the hydrogel can be rapidly adapted via selective photochemical dimerization of stilbazolium within CB[8], leading to IPNs with increased form stability while retaining the dynamic nature of the hydrogels. This modular approach opens new design opportunities for extrudable and cell-friendly dynamic biomaterials for applications in 3D-bioprinting.

1. Introduction

In the past decades, the precise printing of biologically active constructs across various length scales has become an important part of tissue engineering and regenerative medical research.[1] Tremendous success has been achieved in both improving printing techniques and formulating suitable aqueous biomaterials to encapsulate cells.[2,3] In a typical procedure using extrusion-based bioprinting, a cell-laden material is extruded through a nozzle to form filaments that fabricate 3D architectures by overlapping multiple layers of filaments. It is remarkably challenging to develop a bioink that fulfill the requirements in terms of its physical, chemical, and biochemical properties such as cytocompatibility, viscoelasticity, shear-thinning, and self-healing behavior as well as shape fidelity.[4] Besides the usage of naturally derived biopolymers such as hyaluronic acid,[5] alginate,[6] gelatin,[7] and collagen,[8] there is growing interest in synthetic hydrogels made of pluronics,[9] poly(ethylene glycol) (PEG),[10] poly(*N*-isopropylacrylamide)[11,12] as well as poly(2-oxazoline-*co*-2-oxazine).[13,14]

Compared to a hydrogel based on a single synthetic polymer, the native extracellular matrix (ECM) is complex and dynamic. To better emulate the native ECM microenvironment, supramolecular hydrogels are emerging as promising candidates for the application as bioinks.[1] Driven by their noncovalent crosslinking mechanisms, supramolecular hydrogels exhibit softness, viscoelasticity, shear-thinning, and dynamic behavior.[3] Along with the reversible physical crosslinking, the hydrogel can rearrange itself and adapt to the cells during growth. Given by the profound impact of matrix stiffness and the material stress relaxation on cell behavior,[15–18] rheological properties are considered as critical parameters in bioink design.[19]

Recent advancements were made in the development of supramolecular bioinks based on polypeptide hydrogels,[20,21] polypeptide–DNA complexes,[22] hydrogels with DNA crosslinks,[23] and hydrogels crosslinked by host–guest complexation.[24,25] To overcome the low viscosity and the lack of print fidelity, post-printing modifications are engineered

Y. Wang, A. M. Bimmermann, P. Besenius
Department of Chemistry
Johannes Gutenberg University Mainz
Duesbergweg 10–14, 55128 Mainz, Germany
E-mail: y.wang@uni-mainz.de; besenius@uni-mainz.de
M. Neufurth
Institute for Physiological Chemistry
University Medical Center Mainz
Duesbergweg 6, 55128 Mainz, Germany

The ORCID identification number(s) for the author(s) of this article can be found under https://doi.org/10.1002/adma.202313270

DOI: 10.1002/adma.202313270

into the hydrogel systems to stabilize the 3D structures and prevent the dissolution of the gel under wet conditions as in most biomedical applications. To address these issues, interpenetrating network (IPN) formation[25–28] became a popular and promising approach. In a typical procedure, the IPN is formed using different crosslinking reactions to create one flexible primary network and one stiff secondary network that have limited interactions with each other.[1] For this purpose, photochemical polymerization using visible light is commonly conducted for secondary network formation after the printing process to increase the stiffness of printed constructs.[24,29] However, the curing process is often too slow due to randomly distributed network components to be suitable for 3D-bioprinting. The application of an external light source can also cause damage of the cells.[30]

One effective and selective supramolecular cross-linking mechanism is to involve host–guest inclusion complexes. Cucurbit[*n*]urils (n = 5–9 or 10; CB[*n*]) are a family of macrocycles each composed of n methylene-linked glycoluril monomers.[31] In particular, cucurbit[8]uril (CB[8]) has a larger cavity size compared to the smaller homologs enabling the inclusion of two molecules to form either a 2:1 homoternary or a 1:1:1 heteroternary complex with high affinities (K_{eq} up to 10^{14} M^{-2}),[31,32] which makes it attractive for the design of supramolecular polymeric materials.[33,34] Moreover, cucurbiturils are widely exploited as molecular containers for catalyzed and templated chemical reactions.[35] Various examples are reported for oxidation,[36] photodimerization[37,38] and photofragmentation.[39] In the context of CB[8], the formation of the ternary complex leads to a specific spatial arrangement of two reaction components, resulting in enhanced reaction efficiency and selectivity.[40]

In the present study, we report a novel approach utilizing supramolecular IPN hydrogels with tunable physical and chemical crosslink densities for 3D-bioprinting. Therefore, star-shaped PEG is end-functionalized with either tripeptide phenylalanine-glycine-glycine (FGG) or stilbazolium iodide (SB) to obtain polymers PEG-FGG and PEG-SB. Both end groups can undergo supramolecular homoternary host–guest complexation with cucurbit[8]uril, facilitating the formation of three-dimensional single networks (SN) by mixing the functionalized polymers and CB[8] in aqueous media (**Figure 1A**).[40–42] Notably, the physical network with stilbazolium as a guest molecule can be further transformed into a chemical network with high efficiency in a photochemical [2+2]-cycloaddition.[43] By combining both networks, we demonstrate the capability to finely tune the ratio between the supramolecular and covalent networks after a short irradiation period. It enables us to control the network relaxation and stiffness of the hydrogels, thereby enhancing the print fidelity while maintaining the extrudability and self-healing properties. As a result, an additional irradiation step for post-printing processing is not necessary, which is beneficial in working with cell cultures. In contrast to conventional IPNs with randomly distributed secondary network monomers,[1] both networks in our study are formed simultaneously following the same supramolecular cross-linking mechanism in the first stage (Figure 1B). Subsequently, the irradiation step leads to a rapid and selective transformation of the stilbazolium-based dynamic network into a covalent static network due to the pre-organization, resulting in faster covalent network formation and higher homogeneity in the network structure. Using rheology measurements, we investigated the mechanical properties of the hydrogels before and after the irradiation. We further measured UV–Vis spectra of stilbazolium iodide to gain insights into the photochemical dimerization kinetics in cases with or without the CB[8] host molecule as reaction template. Finally, we assessed the cytocompatibility and post-printing stability of the IPN hydrogel through cell viability assays, bioprinting experiments and mineralization assays with osteoblastic SaOS-2 cell line, aiming for the application of our IPN hydrogels as a biomaterial ink for 3D-bioprinting and bone tissue regeneration (Figure 1C).

2. Results and Discussion

2.1. Design and Synthesis of Functional Network Building Blocks

In this work, two different functionalized polymers are synthesized as network building blocks, one with FGG tripeptide and the other carrying stilbazolium iodide as end groups. Four-arm poly(ethylene glycol) (4arm PEG-OH, M_w = 20 kDa, Đ = 1.02), a water-soluble and biocompatible star-shaped polymer, is chosen as structural component of the supramolecular biomaterial ink. By incorporating CB[8]-binding molecules as end groups, namely phenylalanine-glycine-glycine tripeptide (FGG, **1**) and stilbazolium iodide (SB, **2**), the polymers are able to form three dimensional networks individually upon simple mixing with CB[8] in aqueous media driven by the 2:1 homoternary host–guest complex formation.[40,42] Stilbazolium contains a carbon–carbon double bond which allows the photochemical [2+2]-cycloaddition leading to the formation of a dimer[40,43] (Figure 1C). In the context of the corresponding hydrogel networks, the application of an external light source can rapidly transform the dynamic physical network into a static chemical network.

The synthetic routes for the PEG functionalization shown in **Figure 2** are inspired by the work of Tang.[44] The free hydroxy end-groups of 4arm PEG-OH were converted into *p*-nitrophenyl carbonates using *p*-nitrophenyl chloroformate. The resulting polymers were subjected to a reaction with amine carrying guest molecules (**1** or **2**), leading to the formation of carbamate linkages. In case of the peptide-functionalized PEG, an additional step involving Fmoc-deprotection was achieved using a 20% piperidine solution in DMF. Finally, the polymers were purified via dialysis. The degree of functionalization was calculated in ^{1}H-NMR spectra by comparing the aromatic signals of phenylalanine or stilbazolium to the broad signal associated with the PEG back bone. For both polymers, a degree of functionalization of around 80% was achieved.

2.2. Photoisomerization and Photochemical Dimerization of Stilbazolium Iodide

To explore the role of CB[8] in the photodimerization kinetics, UV–Vis spectroscopic studies were carried out. We prepared aqueous solutions of stilbazolium as small molecule in the absence and presence of CB[8]. Both solutions were prepared in

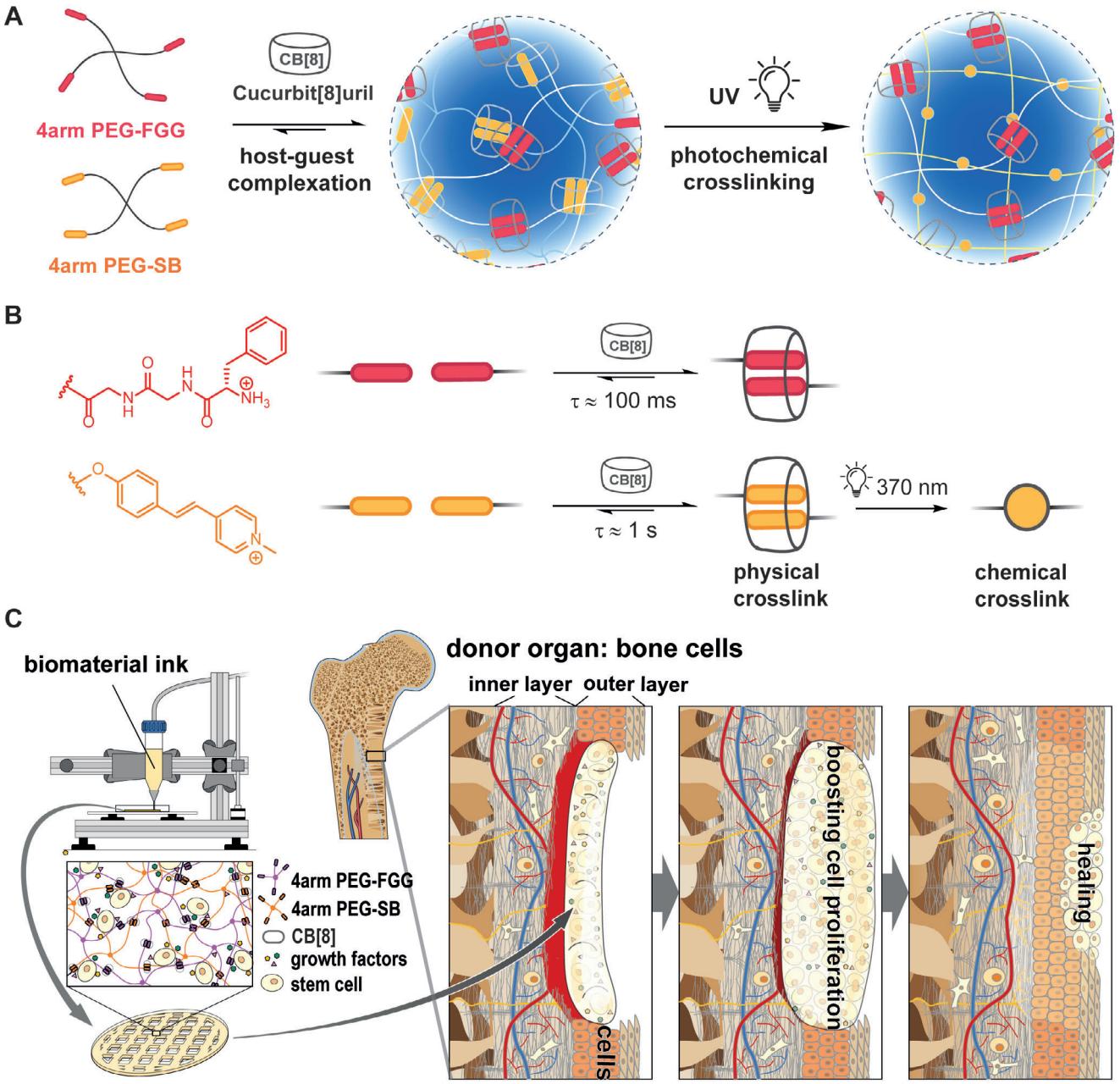

Figure 1. Formation of physical networks following cucurbit[8]uril host–guest interaction and selective transition of one network into a covalent network. The hydrogels formed in this process are potential candidates for dynamic bioinks, especially in the application of bone tissue regeneration. A) Schematic representation of hydrogel formation utilizing functionalized 4arm poly(ethylene glycol) (PEG), PEG-FGG (red), and PEG-SB (yellow). Irradiation with a light source with the wavelength of 370 nm leads to selective transition of the physical network based on PEG-SB into a covalent chemical network. B) Molecular structure of the guest Phe-Gly-Gly tripeptide (FGG) and stilbazolium iodide (SB). Both of them are able to form host-guest complexes by mixing with CB[8] in aqueous media. The physical cross-link formed by stilbazolium iodide and CB[8] can be transformed into a chemical cross-link by the application of a 370 nm light source. C) Application of the interpenetrating network (IPN) hydrogels as biomaterial ink in 3D-bioprinting and in bone tissue regeneration. The printed disc including stem cells can be implanted into a bone defect and support cell proliferation and differentiation, thus promoting bone regeneration.

water containing the same concentration of stilbazolium iodide ($c = 6 \times 10^{-5}$ mol L^{-1}). To one of the solutions, 0.5 mol equivalent of CB[8] was added to achieve a stilbazolium-CB[8] ratio of 2:1. UV–Vis absorption spectra of both solutions reveal an absorption maximum at 370 nm, which was selected as the wavelength for the external light source. The solutions were irradiated using a 370 nm LED, while absorption spectra were measured at various intervals during the irradiation process (**Figure 3**B,C).

In the absence of CB[8], two different photochemical processes are observed, the *cis-trans*-isomerization[45] and the

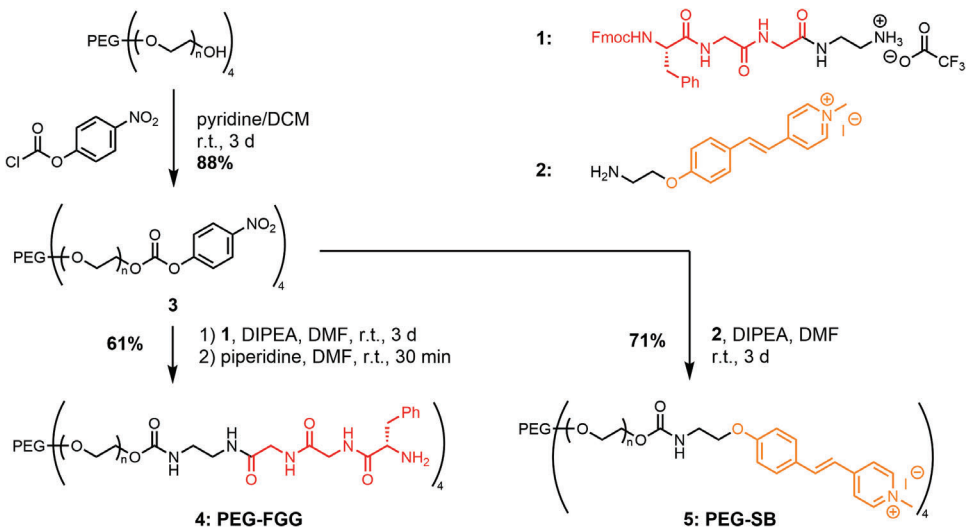

Figure 2. Synthetic routes for functionalization of 20k 4arm PEG-OH with tripeptide FGG (1) or stilbazolium iodide (2).

[2+2]-cycloaddition[40] (as depicted in Figure 3A). At the beginning of the irradiation, the absorption band at 370 nm decreases accompanied by the appearance of a new band at 450 nm. The latter gradually diminishes over extended irradiation durations. Simultaneously, an additional absorption band at 229 nm steadily intensifies over time (Figure 3B). To verify the findings in the UV–Vis spectra, ^{1}H-NMR measurements were conducted across different durations of irradiation (see ESI Figure S16, Supporting Information). We found that the band at 370 nm is associated with the *trans*-isomer of stilbazolium, while the bands at 450 and 229 nm correspond to the *cis*-isomer and the dimer, respectively. This implies that the *trans*-isomer can be converted into the *cis*-isomer upon initial irradiation, while the photodimerization takes place on longer time scales. These findings are in line with the principles of reaction kinetics since the isomerization is a monomolecular process, whereas the dimerization undergoes a bimolecular mechanism.

Interestingly, the introduction of CB[8] into the solution remarkably suppresses the photoisomerization. While the absorption band at 370 nm relating to the *trans*-isomer decreases upon irradiation, an increase of band intensity can be observed exclusively at the wavelength of 229 nm attributed to the dimer formation (Figure 3C). The presence of CB[8] therefore results in a rapid conversion and completion of the dimerization event already after 10 min irradiation. In contrast, the *trans*-isomer is not fully converted into the dimer even after 3 h of irradiation

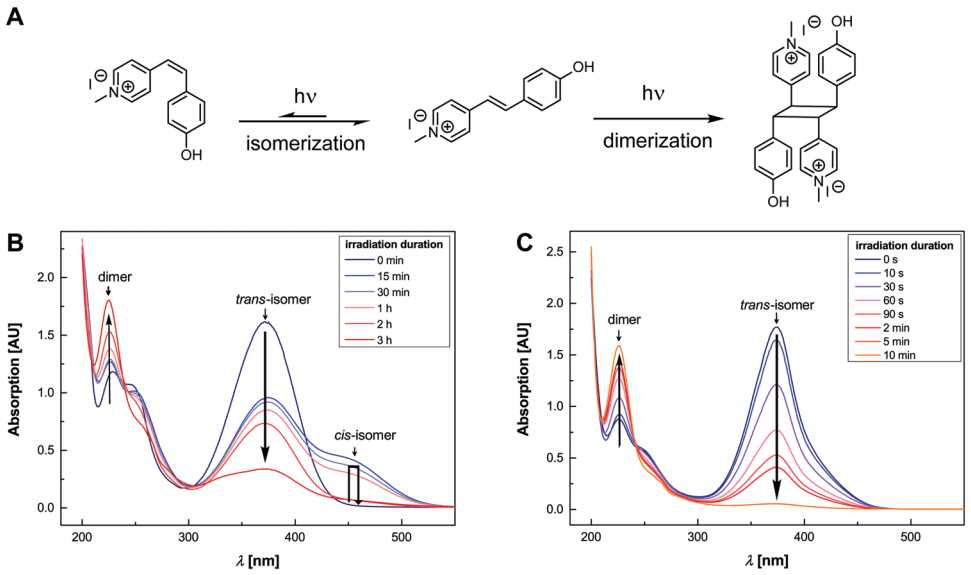

Figure 3. Photoresponsive properties of stilbazolium iodide. A) Stilbazolium iodide (6) can undergo either a *cis-trans*-isomerization or a photochemical dimerization upon irradiation. B) UV–Vis absorption spectra of an aqueous solution containing stilbazolium ($c = 6 \times 10^{-5}$ mol L^{-1}) after different irradiation duration. C) UV–Vis absorption spectra of an aqueous solution containing stilbazolium ($c = 6 \times 10^{-5}$ mol L^{-1}) and CB[8] (0.5 molar equivalent) after different irradiation durations.

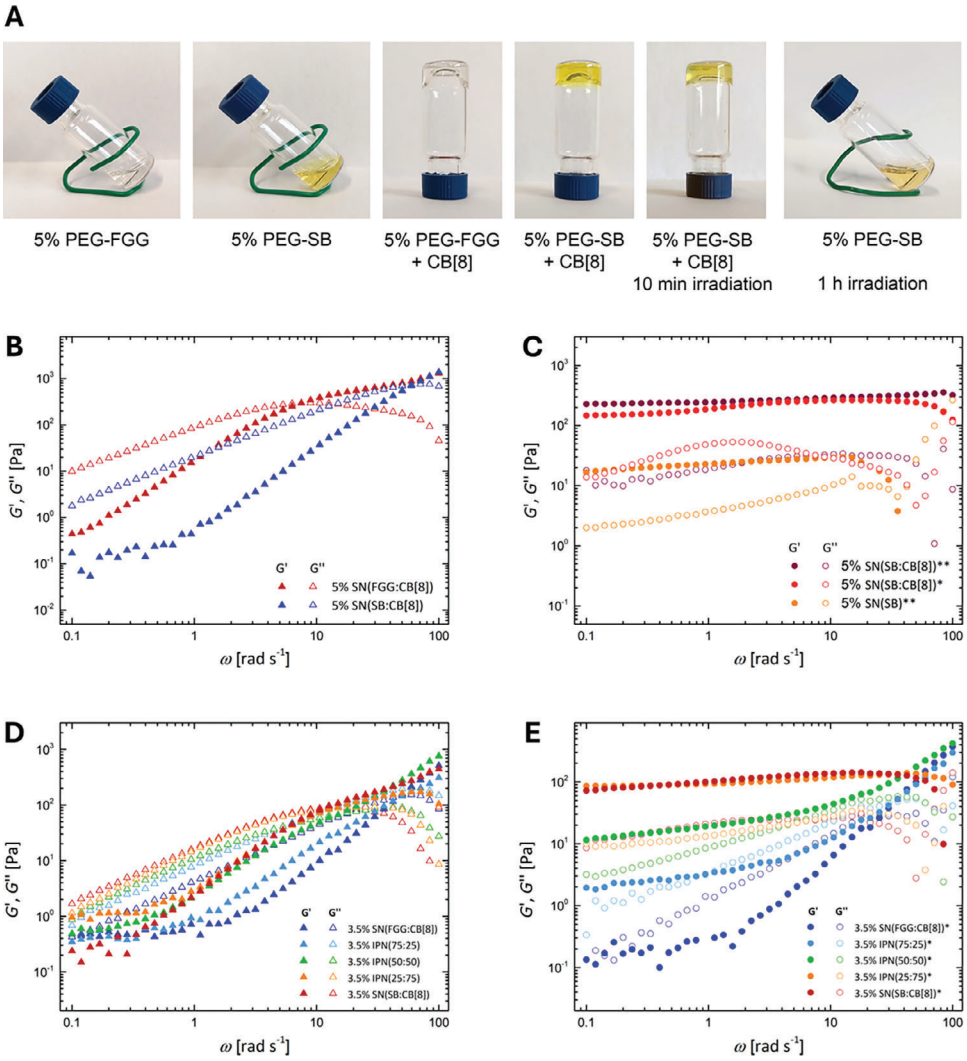

Figure 4. Hydrogel formation of PEG-FGG and PEG-SB with CB[8]. A) Photos of solutions or hydrogels, from left to right: 5 wt% PEG-FGG solution, 5 wt% PEG-SB solution, hydrogel of 5 wt% PEG-FGG crosslinked with CB[8], hydrogel of 5 wt% PEG-SB crosslinked with CB[8], hydrogel of 5 wt% PEG-SB crosslinked with CB[8] after 10 min irradiation, and hydrogel of 5 wt% PEG-SB without CB[8] after 1 h irradiation with a 370 nm LED. B) Frequency sweeps of 5 wt% single network (SN) hydrogels using PEG-FGG (dark blue) or PEG-SB (red) with CB[8] in a molar ratio of 2:1 relating to the end group and CB[8]. C) Frequency sweeps of 5 wt% covalent networks composed of PEG-SB in the presence of CB[8] after irradiation of 1 h (brown) or 10 min (red) and in the absence of CB[8] after irradiation for 1 h (orange). D) Frequency sweeps of 3.5 wt% interpenetrating network (IPN) hydrogels with 0%, 25%, 50%, 75%, and 100% PEG-SB before irradiation. E) Frequency sweeps of 3.5 wt% IPN hydrogels with 0%, 25%, 50%, 75%, and 100% PEG-SB after 10 min irradiation with a 370 nm light source.

when the CB[8] host molecule is absent. Evidently, CB[8] provides a confined space that pre-organizes two stilbazolium molecules within its cavity and forces the reactive pair to dimerize. Translating this phenomenon to a polymeric system where stilbazolium is introduced as end-groups, the complexation of the end-groups with CB[8] can offer an efficient method to transform a dynamic network into a static one just by applying an external light trigger. In comparison to the conventional IPN approach, which features a random distribution of the secondary network monomers throughout the primary network,[3] a pre-organization of the secondary network building blocks can lead to higher efficiency in network formation and increased homogeneity in the resulting network structure, since the network junctions are pre-installed.

2.3. Single Network Formation and Photochemical Network Transformation

To study the characteristics of the SN, 5 wt% hydrogels containing either PEG-FGG or PEG-SB with and without CB[8] in PBS buffer were prepared. Information about sample composition and irradiation duration are summarized in Table S1 (Supporting Information).

By simple addition of CB[8] to the solutions containing 5% of the polymer, hydrogels featuring viscous flow (5% SN(FGG:CB[8])) or solid-like properties (5% SN(SB:CB[8])) are formed (see **Figure** 4A). The binding constants reported for homodimers with CB[8] are $\log(K_{eq}) = 11.17$ in case of the

FGG tripeptide[42] and log(K_{eq}) = 8.00 for stilbazolium,[41] indicating a higher thermodynamic stability for the homoternary complex formed between FGG tripeptide and CB[8]. Surprisingly, the rheological data demonstrate that the SN hydrogel with FGG–CB[8] complexes as crosslinks has a crossover frequency at a higher frequency regime (Figure 4B), relating to faster network relaxation.[46] The network relaxation times derived from the crossover frequencies are τ = 97 ms for the PEG-FGG network and τ = 838 ms for the PEG-SB network, respectively. Since the crosslink densities in both SNs are comparable, the observation reveals that the physical network crosslinked by FGG–CB[8] complexes displays higher exchange rates in terms of complex dissociation and association kinetics.[46] This finding is significant when we consider the relationship between the mechanical properties of the matrix and cell activity.[16] Using FGG–CB[8] complexes as transient crosslinks, the hydrogel will show rapid stress relaxation and viscoelastic liquid-like behavior.

To validate the outcomes of the UV–Vis studies of stilbazolium, photochemically crosslinked hydrogels composed of 5 wt% PEG-SB in the presence and absence of CB[8] were prepared and analyzed through rheological measurements. In the presence of CB[8], a physically crosslinked hydrogel is formed in the first stage and is transformed into a static, covalently crosslinked network upon exposure of 370 nm LED light irradiation (Figure 4A,C). Before the irradiation (Figure 4B, 5% SN(SB:CB[8])), a transition from solution to gel can be observed in the frequency sweep (crossover frequency), typical viscoelastic behavior of physical or supramolecular hydrogels. After 10 min irradiation, the frequency sweep demonstrates the formation of a static hydrogel (5% SN(SB:CB[8])*) and a storage modulus *G'* which is an order of magnitude higher than the loss modulus *G''* across the entire frequency test window. A similar behavior is observed for the hydrogel after 1 h irradiation time (5% SN(SB:CB[8])**). In contrast, when CB[8] is absent, the solution is unable to form a stable gel after 10 min irradiation period (Figure 4A), and only after 1 h irradiation a static hydrogel is obtained (Figure 4C, 5% SN(SB)**). However, in absence of CB[8], the storage modulus *G'* is only around 10 Pa, which is approximately one order of magnitude lower compared to the hydrogel formed in the presence of CB[8] with a storage modulus *G'* around 100 Pa. This is indicative of a higher crosslinking density that is achieved using CB[8] mediated photodimerization. The kinetic investigations and rheological characterization demonstrate that the pre-organization of the stilbazolium end groups through host–guest complexation with CB[8] provides a promising methodology for efficient photochemical crosslinking.

2.4. Interpenetrating Network Formation

By mixing both polymer components with CB[8], we aim to create IPN hydrogels with tunable physical and chemical crosslink densities, leading to materials with adjustable (bio-)mechanical properties encompassing stiffness, viscoelasticity, and self-healing behavior. To explore those properties, we prepared hydrogels with 3.5 wt% polymer content (PEG-FGG with varying fractions of PEG-SB: 0%, 25%, 50%, 75% or 100%) and CB[8] in a ratio of 2:1 with respect to the polymer end groups to CB[8].

Before irradiation, all hydrogels contain only physical crosslinks by homoternary host–guest complexation of the polymer end groups with CB[8]. The measured frequency sweeps (Figure 4D) reveal similar viscoelastic behavior for all gel compositions, with slight shifts of the crossover frequency towards lower frequency ranges with increasing amount of PEG-SB, which was expected from the experiments on the individual hydrogels of 100% PEG-FGG and 100% PEG-SB, respectively. Upon irradiation with a 370 nm LED, the hydrogels exhibit substantial changes in mechanical properties. Frequency sweeps of the respective hydrogels are shown in Figure 4E. The hydrogel containing 25% PEG-SB (3.5% IPN(75:25) in Figure 4D) exhibits similar viscoelastic liquid-like behavior as the pure 100% PEG-FGG network (3.5% SN(FGG:CB[8]) in Figure 4D). However, after 10 min irradiation (3.5% IPN(75:25)* in Figure 4E), the storage modulus *G'* is higher than the loss modulus *G''* in the lower frequency regimes compared to the pure physical gel, implying a small solid-like contribution of the chemical network originating from dimerized stilbazolium species. In contrast, the behavior of the hydrogel comprising 75% PEG-SB (3.5% IPN(25:75)* in Figure 4E) is dominated by the photochemically crosslinked network, resulting in a solid-like material (storage modulus *G'* higher than loss modulus *G''*) over the entire frequency spectrum. Further information to network relaxation time and plateau modulus are summarized in Table S2 (Supporting Information).

Intriguingly, the hydrogel made from a polymer ratio of 1:1 (3.5% IPN(50:50)* in Figure 4E) displays an intermediate behavior demonstrating solid-like attributes without being entirely static. At low frequencies, the hydrogel exhibits characteristics of the chemical network, whereas features of the transient physical network are demonstrated in the higher frequency range. This indicates that the form stability of the hydrogels is improved through the formation of a covalent network, while the dynamic nature related to the supramolecular host–guest complexation is maintained.

In the context of bioprinting, both mechanical support and dynamics of the biomaterial inks are significant not only in terms of their extrudability[4] but also with respect to their impact on cell behavior.[16,17] Therefore, the dynamic properties of the IPN hydrogels were further investigated in terms of stress relaxation of the material. By applying a constant strain of 10% to the hydrogel, we observed different stress relaxation behavior depending on the gel composition and preparation (**Figure 5**A). Since the formation of host–guest complexes is reversible, physically crosslinked single and IPNs (3.5% SN(FGG:CB[8]), SN(SB:CB[8]) and IPN(50:50)) show full relaxation within 1 s due to the disassembly of the network. In case of a chemically cross-linked hydrogel (3.5% SN(SB:CB[8])*), the stress relaxation with $t_{1/2}$ = 20 s results from rearrangements of the polymer chains between network junctions. When a strain is applied to the hydrogel containing 50% physical and 50% chemical cross-links (3.5% IPN(50:50)*), the relaxation of the initial stress is induced by both mechanisms, leading to faster relaxation ($t_{1/2}$ = 2 s) compared to the fully covalent network, closely resembling that found in biological tissues.[47]

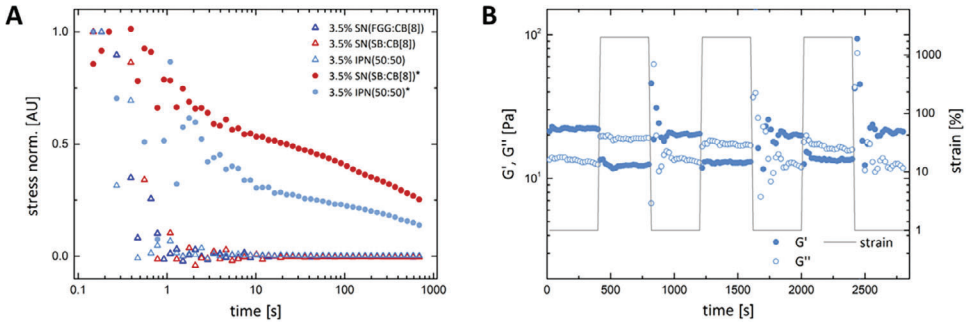

Figure 5. Dynamic properties of the hydrogels. A) Stress relaxation of 3.5% hydrogels composed of single network (SN) or interpenetrating network (IPN) crosslinked with CB[8] before and after 10 min irradiation with an external light source of 370 nm. The measurements were performed at a constant strain of 10%. B) Step-strain measurement of 3.5% IPN(50:50)* with alternating strain between 1% and 2000%.

Furthermore, compression testing was carried out to assess the processability of the hydrogels with respect to compressive loading.[48] The compression stress–strain curves are shown in Figure S17 (Supporting Information). Compressive moduli E_{comp} for different irradiated gel samples were calculated and summarized in Table S2 (Supporting Information). For 3.5% hydrogels with 50%, 75%, and 100% PEG-SB, the compression modulus slightly increases from (1.14 ± 0.04) to (2.34 ± 0.95) kPa with increasing percentage of the chemical crosslink. By changing the polymer concentration from 3.5% to 5%, the compression modulus significantly increases to (9.46 ± 0.58) kPa, indicating that the polymer concentration has a higher influence on the compressive properties of the hydrogels than the type of crosslink.

To investigate the printability, flow curves with increasing shear rates from 0.01 to 1000 s^{-1} were measured for different SN and IPN hydrogels (see Figure S18, Supporting Information). All hydrogels tested show shear-thinning behavior. In addition, a step-strain measurement (alternating strain between 1% and 2000%) was performed for the IPN hydrogel 3.5% IPN(50:50)* to study the shear-thinning and self-healing behavior (Figure 5B). While the gel exhibits solid-like behavior ($G' > G''$) at 1% strain, the hydrogel becomes a liquid ($G'' > G'$) when 2000% strain is applied due to disassembly of the noncovalent network. When the strain is decreased to 1%, the gel recovers rapidly which is realized by the reversibility of the host–guest complexes between the FGG tripeptide and CB[8]. Applied to the bioprinting experiment, our IPN hydrogel is able to transform into a liquid when passing through the nozzle, and restore its stiffness directly after the extrusion process.

2.5. Cell Culture Experiments and Bioprinting

In the development of a biomaterial ink, requirements towards mechanical properties such as matrix stiffness and viscoelasticity should be fulfilled. The stiffness of the hydrogel plays an important role in providing structural support for cells and maintaining the print shape post-extrusion. At the same time, the hydrogel should exhibit dynamic and viscoelastic features to be able to respond to the cell growth. To address these requirements, we chose the photochemically crosslinked IPN with 50% PEG-FGG as a dynamic component and 50% PEG-SB as structural component.

Cell viability assay was carried out using SaOS-2 cell line to assess the cytocompatibility of the hydrogel. The cells were mixed with different amounts of the hydrogel (0, 3, 10, 30 µL) and cultivated for 3 days. After addition of the membrane penetrating calcein-AM stain,[49] the cell viability was calculated from the fluorescence intensity with respect to the control experiment (with 0 µL addition of gel). The results (shown in **Figure 6A**) reveal that our IPN hydrogel is nontoxic and applicable to encapsulate cells.

We further want to explore the potential in 3D-bioprinting applications. To achieve this, 3.5 wt% IPN hydrogel preloaded with cell suspension was prepared and subjected to extrusion-based bioprinting experiments. We were able to print robust 2-layer porous cylindrical scaffolds with different sizes (one with a 50 mm diameter and 320 µm layer thickness is shown in Figure 6B). The constructs obtained were covered by cell culture medium and the print stability was assessed after 2 days of incubation (Figure S20, Supporting Information). The cell behavior within the printed scaffolds was evaluated at different incubation times (8, 24, 48, and 72 h) after the extrusion process through the usage of calcein-AM stain solution (Figure 6C). The images show a rounded cell morphology 8 h post-extrusion, while the cells assume more elongated morphology with extended incubation time, enabling the fibroblasts to interconnect to each other.[50] Concurrently, the cell density within the gel matrix exhibited a progressive increase over time (see Figure S19, Supporting Information), indicating that the IPN hydrogel used in the printing experiment is cell-friendly and supports cell proliferation and growth post-extrusion.

The differentiation of SaoS-2 cells within printed constructs was evaluated using in vitro mineralization assays (Figure 6D). Printed discs were covered with cell medium both with and without the addition of an activation cocktail containing β-glycerophosphate, L(+)-ascorbic acid and dexamethasone.[51] After 2, 4, and 6 days of incubation period, staining reagent was added to examine the formation of hydroxyapatite deposited on the cell surface.[52] The samples incubated with activation cocktail show fluorescent staining at each time point (lower panel in Figure 6D), referring to the ability of SaoS-2 cells to differentiate in the given IPN gel matrix after the printing event.

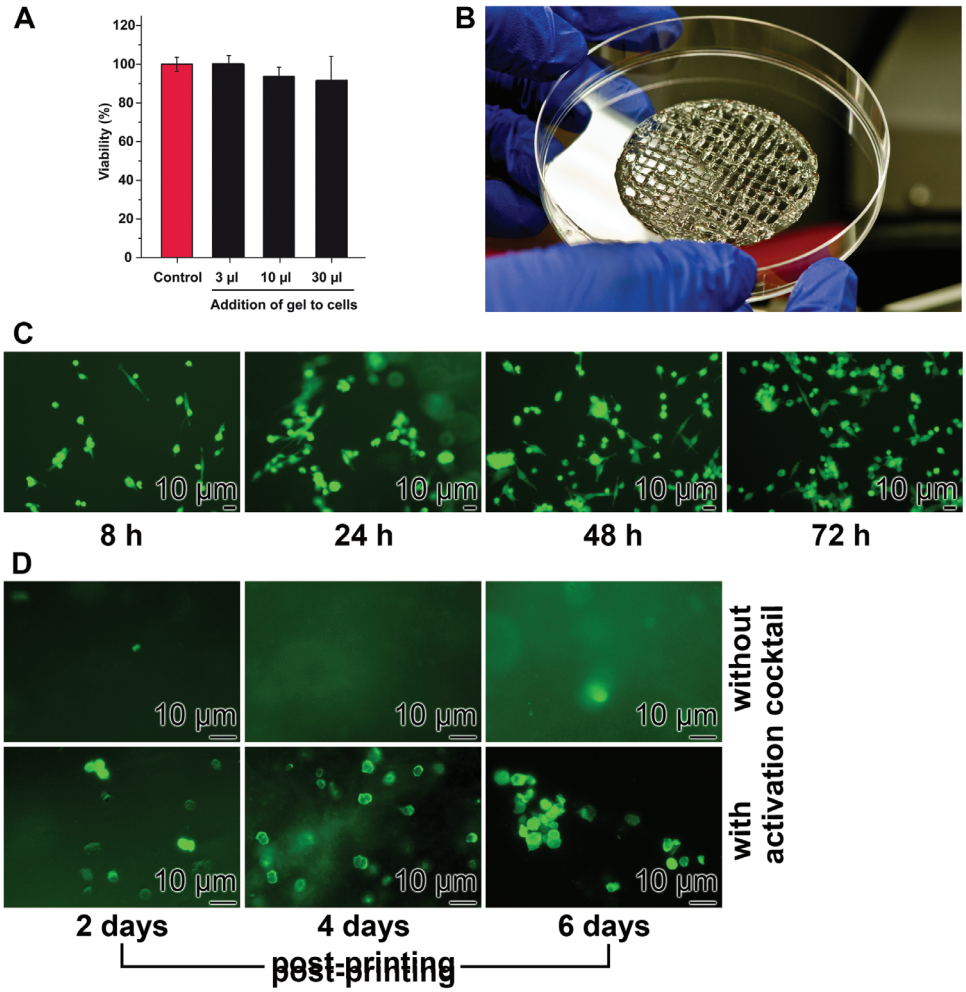

Figure 6. Cell viability and bioprinting. A) Cell viability assay of 3.5 wt% photochemically crosslinked hydrogel with a polymer ratio of 1:1. The bars demonstrate the viability of cells after 3 days of cultivation with addition of the hydrogel (0, 3, 10, 30 µL from left to right). The error bars refer to standard deviations. B) Cylindrical disc printed with cell-laden 3.5 wt% pre-crosslinked hydrogel. C) Cell viability was evaluated to 8, 24, 48, and 72 h post-extrusion utilizing calcein-AM stain. The images were recorded in the fluorescence mode using excitation wavelength of 495 nm and emission wavelength of 511 nm. D) The differentiation of the SaoS-2 cells post-printing was assessed using a mineralization assay. Printed discs were cultivated in parallel with and without the activation cocktail. The mineral depositions on the cell surface were stained after 2, 4, and 6 days post-printing. The images were recorded in the fluorescence mode using excitation wavelength of 492 nm and emission wavelength of 520 nm.

3. Conclusions

In this work, we have demonstrated a supramolecular IPN design based on cucurbit[8]uril host–guest interactions with Phe-Gly-Gly tripeptide and stilbazolium iodide as guest molecules. By simply mixing the polymers with CB[8] in aqueous media, physical networks with fast relaxation are formed in the first stage. Through the application of an external light-stimulus, the SN based on stilbazolium–CB[8] complexes can be rapidly and selectively transformed into a robust covalent network. This remarkable ability allows fine modulation of both the physical and chemical crosslinking densities, thereby enabling precise control over hydrogel properties in terms of stiffness, viscoelasticity, stress relaxation, and self-healing. Further investigations into the photodimerization kinetics have yielded compelling insights, revealing CB[8] as a reaction template which drastically enhances the reaction rate comparing to the case without precomplexation with CB[8]. Furthermore, the hydrogel constructs exhibit high cytocompatibility, post-extrusion cell viability, and differentiation which opens up new material design opportunities, particularly in the field of 3D-bioprinting.

4. Experimental Section

Materials: Chemicals and (anhydrous) solvents were obtained from commercial sources and used without further purification. All reactions were conducted in oven dried laboratory glass ware. Reaction conditions such as vacuum and argon atmosphere were achieved by the usage of a Schlenk line. Water used for reactions, sample preparation, and high-performance liquid chromatography was purified utilizing a Veolia PURELAB flex 4 (Paris, France) water purification system. Acetonitrile for high performance liquid chromatography was purchased commercially in HPLC grade. Spectra/por biotech cellulose ester dialysis membranes (VWR, diameter = 20 mm, MWCO = 0.1–0.5 kDa) were purchased from

VWR and used as received. For cell culture, McCoy's medium and fetal calf serum (FCS) were purchased from Biochrom-Seromed (Berlin, Germany) and calcein-AM solution (Sigma–Aldrich) was used as staining reagent for cell viability evaluations. In the mineralization assay, β-glycerophosphate, L(+)-ascorbic acid and dexamethasone (Sigma–Aldrich) were used for the induction of mineralization and the mineral depositions were stained with OsteoImage-Mineralization Assay (Lonza, Köln, Germany).

UV–Vis Spectrometry: UV–Vis spectra were recorded on a PerkinElmer Lambda 365+ (Waltham, USA) UV–Vis spectrometer utilizing a tungsten-halogen and a deuterium lamp at 20 °C. Without CB[8]: 1.0 mg (*E*)-4-(4-hydroxystyryl)-1-methylpyridin-1-ium iodide (**6**) was dissolved in 50 mL water ($c = 6 \times 10^{-5}$ mol L^{-1}) and shaken thoroughly. An amount of 20 mL were transferred into a glass vial equipped with a magnetic stirrer for good mixing. The sample was irradiated using the same 370 nm LED mentioned above. The UV–Vis absorption spectra from 200 to 500 nm were recorded after irradiation duration of 0 min, 15 min, 30 min, 1 h, 2 h, and 3 h. With CB[8]: 1.0 mg (*E*)-4-(4-hydroxystyryl)-1-methylpyridin-1-ium iodide was dissolved in 50 mL water ($c = 6 \times 10^{-5}$ mol L^{-1}) and 1.8 mg (0.5 eq.) CB[8] were added. The mixture was shaken thoroughly and irradiated with ultrasonic radiation for one minute. Each measurement was performed with a different sample, containing 5 mL of the mixture. The sample was irradiated using the same 370 nm LED. The UV–Vis absorption spectra from 200 to 500 nm were recorded after irradiation duration of 0 s, 10 s, 30 s, 60 s, 90 s, 3 min, 5 min, and 10 min.

Hydrogel Preparation: Stock solutions of polymers PEG-FGG and PEG-SB with a concentration of 35 mg mL^{-1} were prepared by dissolving the polymer in PBS buffer. Respective amounts of the stock solutions were mixed in mass vials to obtain 150 µL solutions containing 0%, 25%, 50%, 75%, and 100% component PEG-SB. After the addition of CB[8] (1 mg), the samples were vortexed and shaken at 40 °C overnight under exclusion of light.

Photochemical Crosslinking of PEG-SB Network: In transparent Eppendorf 1.5 mL safe-lock tubes, 60 µL gel samples containing 0%, 25%, 50%, 75%, and 100% component PEG-SB were prepared following the procedure above. The hydrogels were each irradiated for 10 min using a Kessil PR160L-370 nm (Richmond, Canada) LED under the maximal intensity of 399 mW cm^{-2} in 1 cm distance for photochemical crosslinking of the PEG-SB network. Each sample was placed 10 cm relative to the lamp and irradiated for 10 min.

Rheology: Mechanical properties of the hydrogel pre- and post-irradiation were studied using a stress-controlled MCR 302e rheometer from Anton Paar (Ostfildern-Scharnhausen, Germany) with a 10 mm diameter parallel-plate measuring system on a silica glass plate (0.05 mm gap). Oscillatory frequency sweeps (0.01–100 rad s^{-1} at a fixed strain of 2%) were performed at 20 °C to measure storage (*G'*) and loss modulus (*G''*) of the hydrogel and to determine the crosslink lifetime of associative network from the crossover frequency ω using the equation $\tau = 1/\beta = 2\pi/\omega$ (β as the network relaxation rate).[46] Amplitude sweeps (0.01–100% strain at a constant angular frequency of 5 rad s^{-1}) were measured at 20 °C to characterize the nonlinear viscoelastic properties. The stress relaxation of individual hydrogels was investigated at a fixed strain of 10%. Flow curves were performed with increasing shear rate $\dot{\gamma} = 0.01$–$1000\ s^{-1}$. Step-strain experiments were carried out to show shear-thinning and self-healing behavior by alternating the strain between 1% and 2000% at an angular frequency of 1 rad s^{-1}.

Compression Tests: Compression tests were carried out using the same rheometer as described above. Therefore, cylindrical hydrogel samples with 10 mm diameter and a thickness between 2.3 and 2.5 mm were prepared in vials following the hydrogel preparation procedure. After photochemical cross-linking using a 370 nm LED (10 min irradiation), the sample was compressed with a velocity of 0.05 mm s^{-1}. The compression modulus (E_{comp}) was calculated using the initial slope of the stress–strain curve. For each sample composition, the experiment was performed three times and the average values and standard deviations are reported.

Cell Culture Conditions: SaOS-2 cells (human osteogenic sarcoma cells) were purchased (#89050205; Sigma) and used for all cell culture experiments. The cells were cultivated in McCoy's medium containing 2×10^{-3} M L-glutamine, and gentamycin (50 mg mL^{-1}), with addition of 10% fetal bovine serum (FCS) in 25 cm^2 flasks or multiwell plates (Orange Scientifique, Brainel'Alleud; Belgium) in a humidified incubator (37 °C and 5% CO_2). The cells were seeded at a starting concentration of 10^5 cells mL^{-1} in 25 cm^2 flasks. Culture medium/FCS was changed every 3 days.

Cell Viability Studies: The viability of SaOS-2 cells (human osteogenic sarcoma cells) was evaluated using calcein-AM labeling following the procedure from Bratosin.[49] After washing with 10 mL PBS, the cells were detached from the flask by addition of 3 mL Trypsin-EDTA solution. After 6 min incubation at 37 °C, an aliquot was taken and added to fresh McCoy medium with 10% FCS to prepare a cell suspension with a concentration of 10^4 cells mL^{-1}. In a 96-well plate, 170 µL cell suspension was mixed with 0, 3, 10, and 30 µL of the testing material respectively and filled up with medium to reach a total volume of 200 µL. After incubation for 72 h, the solution was removed, and the cells washed with PBS. After addition of 200 µL of 0.15% calcein-AM stain solution in each well and 15 min incubation, the cell viability was inspected on an Olympus IX71 fluorescence microscope using the excitation wavelength of 495 nm and emission wavelength of 511 nm. Vital cells were detected in green. For each hydrogel amount, 10 parallel experiments were performed. The results are given as mean values with standard deviation in percentage with respect to the controls.

Bioink Preparation and Bioprinting: Following the protocol in hydrogel preparation, 4 mL of 3.5 wt% hydrogel with PEG-FGG:PEG-SB ratio of 1:1 was prepared and irradiated 10 min using a 370 nm LED for photochemical cross-linking of the PEG-SB network. To the pre-crosslinked hydrogel, 200 µL of cell suspension (10^5 cells mL^{-1}) was added and the mixture was loaded to a sterile 30 mL cartridge. The bioprinting experiments were performed on a computer-controlled 3D-Bioplotter (4th generation 3D-bioplotter) from EnvisionTEC GmbH (Gladbeck, Germany). The cartridge containing the bioink was connected with a steel needle and placed in a temperature controlled printing head. The printing process was carried out at a temperature of 11 °C with a pressure of 2.0 bar and a printing speed of 8 mm s^{-1}. Cylindrical constructs with diameters of 10 or 50 mm diameter and 320 µm layer thickness were directly injected into 94 mm petri dishes (Greiner Bio-One, Frickenhausen, Germany).

Evaluation of Print Fidelity: To evaluate the print stability, a 2-layer printed disc was fully covered by McCoy's medium with 10% FCS and incubated at 37 °C.

Cell Viability Post-Extrusion: Printed discs containing SaOS-2 cells were incubated for indicated time periods. The cell viability and growth were assessed using calcein-AM stain as described in cell viability studies to 8, 24, 48, and 72 h post-extrusion. In addition, the total and dead cell numbers directly after seeding as well as 2, 4, and 6 days post-extrusion were quantified using the ReadyProbes Cell Viability Imaging Kit (Thermo Fischer Scientific, Darmstadt, Germany) following the procedure from Whitehead.[53] To the cell culture medium, 50 µL mL^{-1} of the reagent mixture containing NucBlue (for staining of all the cells) and propidium iodide (for dead cells) were added. After incubation for 30 min, the cells were inspected on an Olympus IX71 fluorescence microscope using the excitation wavelength of 360 nm and emission wavelength of 460 nm for the detection of NucBlue (excitation at 360 nm, emission at 469 nm) and propidium iodide (excitation at 535 nm, emission at 617 nm).

Mineralization Assay: The differentiation of SaOS-2 cells post-printing was investigated by induction of the inorganic hydroxyapatite formation. Printed discs containing SaOS-2 cells were incubated in petri dishes covered by McCoy's medium with 10% FCS at 37 °C. After 6 h, the medium was replaced by fresh McCoy's medium with 10% FCS containing the activation cocktail (5×10^{-3} M β-glycerophosphate, 50×10^{-3} M L(+)-ascorbic acid and 10×10^{-9} M dexamethasone). After incubation of 2, 4, and 6 days, the mineral depositions on the cell surface were stained using the OsteoImage-Mineralization Assay.[52] Fluorescence images were taken with an Olympus IX71 fluorescence microscope using the excitation wavelength of 492 nm and emission wavelength of 520 nm.

Supporting Information

Supporting Information is available from the Wiley Online Library or from the author.

Acknowledgements

Y.W. was financially supported by the Fonds der Chemischen Industrie (Kekulé Fellowship). Funding from the DFG (Deutsche Forschungsgemeinschaft) is acknowledged: P.B. is member of the GRK 2516 (project No. 405552959) and Y.W. is an associate PhD student of the GRK 2516; P.B. is a member of the SFB 1551 (project No. 464588647). The authors are grateful for financial support by the European Research Council (ERC) under the European Union's Horizon 2020 research and innovation program (ERC CoG SUPRAVACC 819856) [Y.W., A.M.B., P. B.]. The authors thank Dr. Shunfeng Wang (University Medical Center Mainz, Germany) for his help on cell culture and Michael Plenikowski (University Medical Center Mainz, Germany) for his inspirations in designing the graphics. [Correction added on April 09, 2024, after first online publication: All figures has been updated.]

Open access funding enabled and organized by Projekt DEAL.

Conflict of Interest

The authors declare no conflict of interest.

Author Contributions

Y.W. and A.M.B. performed the synthesis and rheological experiments. A.M.B. performed the UV–Vis and NMR studies and processed the data. Y.W. performed the cell viability experiments. Y.W. and M.N. carried out the bioprinting experiments and evaluated the data. P.B. supervised the project. Y.W. and P.B. wrote the manuscript.

Data Availability Statement

The data that support the findings of this study are available in the supplementary material of this article.

Keywords

bioprinting, host–guest complexation, interpenetrating network hydrogels, photoresponsive biomaterials, supramolecular chemistry

Received: December 6, 2023
Revised: March 25, 2024
Published online: April 5, 2024

[1] D. Chimene, K. K. Lennox, R. R. Kaunas, A. K. Gaharwar, *Ann. Biomed. Eng.* **2016**, *44*, 2090.
[2] H. Ravanbakhsh, V. Karamzadeh, G. Bao, L. Mongeau, D. Juncker, Y. S. Zhang, *Adv. Mater.* **2021**, *33*, 2104730.
[3] F. L. C. Morgan, L. Moroni, M. B. Baker, *Adv. Healthcare Mater.* **2020**, *9*, 1901798.
[4] M. Hospodiuk, M. Dey, D. Sosnoski, I. T. Ozbolat, *Biotechnol. Adv.* **2017**, *35*, 217.
[5] J. Hauptstein, L. Forster, A. Nadernezhad, J. Groll, J. Teßmar, T. Blunk, *Int. J. Mol. Sci.* **2022**, *23*, 924.
[6] C. C. Piras, D. K. Smith, *J. Mater. Chem. B* **2020**, *8*, 8171.
[7] W. Shi, M. Sun, X. Hu, B. Ren, J. Cheng, C. Li, X. Duan, X. Fu, J. Zhang, H. Chen, Y. Ao, *Adv. Mater.* **2017**, *29*, 1701089.
[8] W. J. Kim, C. H. Jang, G. H. Kim, *Nano Lett.* **2019**, *19*, 8612.
[9] M. Müller, J. Becher, M. Schnabelrauch, M. Zenobi-Wong, *Biofabrication* **2015**, *7*, 035006.
[10] Z. Zheng, J. Wu, M. Liu, H. Wang, C. Li, M. J. Rodriguez, G. Li, X. Wang, D. L. Kaplan, *Adv. Healthcare Mater.* **2018**, *7*, 1701026.
[11] M. Kesti, M. Müller, J. Becher, M. Schnabelrauch, M. D'Este, D. Eglin, M. Zenobi-Wong, *Acta Biomater.* **2015**, *11*, 162.
[12] A. M. Navara, Y. S. Kim, Y. Xu, C. L. Crafton, M. Diba, J. L. Guo, A. G. Mikos, *Bioact. Mater.* **2022**, *14*, 302.
[13] L. Hahn, M. Beudert, M. Gutmann, L. Keßler, P. Stahlhut, L. Fischer, E. Karakaya, T. Lorson, I. Thievessen, R. Detsch, T. Lühmann, R. Luxenhofer, *Macromol. Biosci.* **2021**, *21*, 2100122.
[14] T. Lorson, S. Jaksch, M. M. Lübtow, T. Jüngst, J. Groll, T. Lühmann, R. Luxenhofer, *Biomacromolecules* **2017**, *18*, 2161.
[15] A. J. Engler, S. Sen, H. L. Sweeney, D. E. Discher, *Cell* **2006**, *126*, 677.
[16] O. Chaudhuri, L. Gu, D. Klumpers, M. Darnell, S. A. Bencherif, J. C. Weaver, N. Huebsch, H. P. Lee, E. Lippens, G. N. Duda, D. J. Mooney, *Nat. Mater.* **2016**, *15*, 326.
[17] J. Nicolas, S. Magli, L. Rabbachin, S. Sampaolesi, F. Nicotra, L. Russo, *Biomacromolecules* **2020**, *21*, 1968.
[18] M. Diba, S. Spaans, S. I. S. Hendrikse, M. M. C. Bastings, M. J. G. Schotman, J. F. van Sprang, D. J. Wu, F. J. M. Hoeben, H. M. Janssen, P. Y. W. Dankers, *Adv. Mater.* **2021**, *33*, 2008111.
[19] H. L Hernandez, J. W. Souza, E. A. Appel, *Macromol. Biosci.* **2021**, *21*, 2000295.
[20] M. Dai, J. P. Belaïdi, G. Fleury, E. Garanger, M. Rielland, X. Schultze, S. Lecommandoux, *Biomacromolecules* **2021**, *22*, 4956.
[21] Y. Loo, A. Lakshmanan, M. Ni, L. L. Toh, S. Wang, C. A. E. Hauser, *Nano Lett.* **2015**, *15*, 6919.
[22] C. Li, A. Faulkner-Jones, A. R. Dun, J. Jin, P. Chen, Y. Xing, Z. Yang, Z. Li, W. Shu, D. Liu, R. R. Duncan, *Angew. Chem., Int. Ed.* **2015**, *127*, 4029.
[23] Y.-H. Peng, S. K. Hsiao, K. Gupta, A. Ruland, G. K. Auernhammer, M. F. Maitz, S. Boye, J. Lattner, C. Gerri, A. Honigmann, C. Werner, E. Krieg, *Nat. Nanotechnol.* **2023**, *18*, 1463.
[24] C. B. Highley, C. B. Rodell, J. A. Burdick, *Adv. Mater.* **2015**, *27*, 5075.
[25] T. Hu, X. Cui, M. Zhu, M. Wu, Y. Tian, B. Yao, W. Song, Z. Niu, S. Huang, X. Fu, *Bioact. Mater.* **2020**, *5*, 808.
[26] T. Nonoyama, J. P. Gong, *Proc. Inst. Mech. Eng., Part H* **2015**, *229*, 853.
[27] S. Hong, D. Sycks, H. F. Chan, S. Lin, G. P. Lopez, F. Guilak, K. W. Leong, X. Zhao, *Adv. Mater.* **2015**, *27*, 4035.
[28] S. Houben, A. A. Aldana, A. S. Huysecom, W. Mpinganzima, R. Cardinaels, M. B. Baker, L. M. Pitet, *ACS Appl. Polym. Mater.* **2023**, *5*, 1819.
[29] S. Xin, D. Chimene, J. E. Garza, A. K. Gaharwar, D. L. Alge, *Biomater. Sci.* **2019**, *7*, 1179.
[30] J. Adhikari, A. Roy, A. Das, M. Ghosh, S. Thomas, A. Sinha, J. Kim, P. Saha, *Macromol. Biosci.* **2021**, *21*, 2000179.
[31] S. J. Barrow, S. Kasera, M. J. Rowland, J. Del Barrio, O. A. Scherman, *Chem. Rev.* **2015**, *115*, 12320.
[32] J. Lagona, P. Mukhopadhyay, S. Chakrabarti, L. Isaacs, *Angew. Chem., Int. Ed.* **2005**, *44*, 4844.
[33] M. J. Rowland, M. Atgie, D. Hoogland, O. A. Scherman, *Biomacromolecules* **2015**, *16*, 2436.
[34] E. A. Appel, F. Biedermann, U. Rauwald, S. T. Jones, J. M. Zayed, O. A. Scherman, *J. Am. Chem. Soc.* **2010**, *132*, 14251.
[35] K. I. Assaf, W. M. Nau, *Chem. Soc. Rev.* **2015**, *44*, 394.
[36] Y. H. Wang, H. Cong, F. F. Zhao, S. F. Xue, Z. Tao, Q. J. Zhu, G. Wei, *Catal. Commun.* **2011**, *12*, 1127.
[37] M. Pattabiraman, A. Natarajan, L. S. Kaanumalle, V. Ramamurthy, *Org. Lett.* **2005**, *7*, 529.

[38] B. C. Pemberton, R. K. Singh, A. C. Johnson, S. Jockusch, J. P. Da Silva, A. Ugrinov, N. J. Turro, D. K. Srivastava, J. Sivaguru, *Chem. Comm.* **2011**, *47*, 6323.
[39] J. Smitka, A. Lemos, M. Porel, S. Jockusch, T. R. Belderrain, E. Tesařová, J. P. Da Silva, *Photochem. Photobiol. Sci.* **2014**, *13*, 310.
[40] R. Kaliappan, M. V. S. N. Maddipatla, L. S. Kaanumalle, V. Ramamurthy, *Photochem. Photobiol. Sci.* **2007**, *6*, 737.
[41] S. Senler, L. Cui, A. M. Broomes, E. L. Smith, J. N. Wilson, A. E. Kaifer, *J. Phys. Org. Chem.* **2012**, *25*, 592.
[42] L. M. Heitmann, A. B. Taylor, P. J. Hart, A. R. Urbach, *J. Am. Chem. Soc.* **2006**, *128*, 12574.
[43] L. Zou, M. J. Webber, *Chem. Comm.* **2019**, *55*, 9931.
[44] S. Tang, A. Habicht, S. Li, S. Seiffert, B. D. Olsen, *Macromolecules* **2016**, *49*, 5599.
[45] U. Steiner, M. H. Abdel-Kader, P. Fischer, H. E. A. Kramer, *J. Am. Chem. Soc.* **1978**, *100*, 3190.
[46] W. C. Yount, D. M. Loveless, S. L. Craig, *J. Am. Chem. Soc.* **2005**, *127*, 14488.
[47] O. Chaudhuri, J. Cooper-White, P. A. Janmey, D. J. Mooney, V. B. Shenoy, *Nature* **2020**, *584*, 535.
[48] Y. J. Shin, R. T. Shafranek, J. H. Tsui, J. Walcott, A. Nelson, D. H. Kim, *Acta Biomater.* **2021**, *119*, 75.
[49] D. Bratosin, L. Mitrofan, C. Palii, J. Estaquier, J. Montreuil, *Cytometry, Part A* **2005**, *66*, 78.
[50] F. Grinnell, C.-H. Ho, E. Tamariz, D. J. Lee, G. Skuta, *Mol. Biol. Cell* **2003**, *14*, 384.
[51] M. Wiens, X. Wang, U. Schlomacher, I. Lieberwirth, G. Glasser, H. Ushijima, H. C. Schröder, W. E. G. Müller, *Calcif. Tissue Int.* **2010**, *87*, 513.
[52] Y. H. Wang, Y. Liu, P. Maye, D. W. Rowe, *Biotechnol. Prog.* **2006**, *22*, 1697.
[53] A. K. Whitehead, H. H. Barnett, M. E. Caldorera-Moore, J. J. Newman, *Regener. Biomater.* **2018**, *5*, 167.